Chemical Science

ROYAL SOCIETY OF CHEMISTRY

EDGE ARTICLE

View Article Online
View Journal | View Issue

Check for updates

Cite this: *Chem. Sci.*, 2025, **16**, 1948

All publication charges for this article have been paid for by the Royal Society of Chemistry

Received 30th September 2024
Accepted 16th December 2024

DOI: 10.1039/d4sc06633b

rsc.li/chemical-science

Diacetylene-bridged covalent organic framework as crystalline graphdiyne analogue for photocatalytic hydrogen evolution†

Zhiqing Lin,[a] Songyao Dai,[a] Shan Yao,[b] Qia-Chun Lin,[a] Mengying Fu,[a] Lai-Hon Chung, *[a] Bin Han *[b] and Jun He *[a]

Graphdiyne (GDY) alone as a photocatalyst is unsatisfactory because of its low crystallinity, limited regulation of the band gap, weak photogenerated charge separation, *etc.*, and heterojunctioning with other materials is necessary to activate the photocatalytic activity of GDY. Through elaborate design, a diacetylene-rich linker (**S2**) was prepared and employed to construct a crystalline and structurally well-defined GDY-like covalent organic framework (COF, namely **S2-TP COF**) which merges the merits of both COF and GDY to boost the photocatalytic hydrogen evolution reaction (HER). By theoretical prediction on the donor–acceptor (D–A) pair, two other monoacetylene-bridged COFs (**S1-TP COF** and **S3-TP COF**) were prepared for comparison. Exhibiting enhanced separation and suppressed recombination of photogenerated excitons, Pt-photodeposited **S2-TP COF** showed a higher HER rate (10.16 mmol g^{-1} h^{-1}) than the other two non-GDY-like COFs (3.71 and 1.13 mmol g^{-1} h^{-1}). A joint experimental–theoretical study suggests that the appropriate D–A structure for photogenerated charge separation and diacetylene motif as the adsorption site are the key reasons for the boosted HER. This work opens a new avenue for the rational design of COFs as GDY mimics for photocatalytic application.

Introduction

Graphdiyne (GDY), a 2D carbon-based network composed of sp and sp^2 hybridized carbon, was only a fantasy on the theoretical level until the successful preparation of GDY film on copper foil by Li and co-workers.[1] Since this achievement, GDY has been considered a promising platform for various solar-driven applications including the hydrogen evolution reaction (HER), CO_2 reduction reaction (CO_2RR), nitrogen reduction reaction (NRR), light-assisted pollutant degradation, *etc.* because its large porosity, alkyne-rich functionalities and high degree of π-conjugation favor substrate mass transfer, adsorption of metal ions for building active sites, light harvesting and separation/transport of charge carriers.[2,3] Promising as it seems, GDY has an Achilles' heel of a narrow band gap (0.46–1.22 eV) and mostly resorts to forming a binary/ternary heterojunction with other semiconductors (*e.g.*, CdS, g-C_3N_4, TiO_2, *etc.*) for optimal band structures to actualize photocatalysis.[4–7] Even though a few GDY-based single-component photocatalysts have been achieved recently by introducing defects into the GDY net through editing the structure of graphene precursors (*i.e.*, tuning the number of alkyne groups on the aromatic core or heteroatom/functional group substitution),[8–11] the amorphous nature of the as-prepared GDYs is unfavorable for structure–function correlation (*e.g.*, the function of acetylene bridges and how active sites work during photocatalysis). Another challenge comes with the instability of multialkyne monomers (*e.g.* hexaalkynyl benzene) which contributes to the amorphous nature and causes structural uncertainty of the resultant GDY by side reactions.[12,13] So, to keep the strengths and rectify the weaknesses of GDY, it is necessary to develop novel crystalline platforms featuring a continuum of diacetylene functionalities.

Covalent organic frameworks (COFs) are ideal platforms for constructing crystalline porous polymers with rich functionality customization, well-defined structure, high stability, and tunable pores.[14–18] Intriguingly, the high degree of freedom and precision in structural design is especially useful for the integration of diverse functional units. Specifically, building donor–acceptor (D–A) type COFs has emerged as a convenient and effective strategy for high-performance photocatalysts because this approach allows easy band structure tuning and skips external photosensitizers as well as heterojunction formation.[19–21] In this regard, we propose the incorporation of GDY moieties into COFs to be a two-fold approach to keep the

[a]*School of Chemical Engineering and Light Industry, Guangdong University of Technology, Guangzhou 510006, China. E-mail: junhe@gdut.edu.cn; laihonchung@gdut.edu.cn*

[b]*Guangdong Basic Research Center of Excellence for Ecological Security and Green Development, Key Laboratory for City Cluster Environmental Safety and Green Development of the Ministry of Education, School of Ecology, Environment and Resources, Guangdong University of Technology, Guangzhou, 510006, P. R. China. E-mail: hanbin@gdut.edu.cn*

† Electronic supplementary information (ESI) available. See DOI: https://doi.org/10.1039/d4sc06633b

strengths of GDY (*e.g.*, permanent porosity, abundant alkynyl active sites, intensive π-conjugation) on one hand and rectify the weaknesses of GDY (*e.g.*, lack of bandgap tuning, photosensitizing power) on the other hand.

Since the synthesis of diacetylene-bridged COFs is not easy, only a few examples based on 4,4′-(buta-1,3-diyne-1,4-diyl)dianiline (BDA), 4,4′-(buta-1,3-diyne-1,4-diyl)dibenzaldehyde (BD) or dehydrobenzoannulene (DBA) monomers have been reported so far.[22–27] These works indicate that the diacetylene units not only facilitate the separation and transfer of charge carriers, but also suppress reverse charge recombination to improve the D-to-A migration lifetime of charge carriers, thereby enhancing photocatalytic activity. However, the role of diyne units in COFs is still unclear from the mechanistic viewpoint, especially the comparison with monoacetylene analogues. Therefore, it is crucial to design GDY-like COFs with well-defined structures, tunable band gaps, and abundant diacetylene units to unveil the structure–property correlation and develop next-generation GDY-like catalysts.

Herein, we adopted Glaser–Hay coupling to construct a diacetylene-linked triangular triamine linker (**S2**, Scheme S1†) which was allowed to undergo Schiff-base condensation with classical C_3-symmetric 1,3,5-triformylphloroglucinol (TP) to build a GDY-like COF. As a comparison, triamine linkers with monoacetylene of different skeletal lengths were employed to construct analogous networks for follow-up investigation on how diacetylene-based networks beat monoacetylene counterparts using the photocatalytic HER as a model reaction. Joint experimental and theoretical studies suggest that the GDY-like COF works better than monoacetylene-based analogues, which is attributed to the following advantages: (1) construction of optimal D–A junction to enhance light-harvesting ability; (2) the introduction of −C≡C−C≡C− linkages regulates the planarity of the COF for smooth e^- transport, establishes spatial distance between D–A units for extensive separation of electron–hole (e^-–h^+) pairs and minimizes exciton binding energy; (3) the GDY-like COF generates good reactant affinity, improving the loading and dispersion of the Pt cocatalysts, thereby achieving excellent photocatalytic performance. This work presents an unprecedented way to merge the merits of GDY into the structurally robust, diversified crystalline framework for the rational development of functional materials.

Results and discussion

Construction of D–A pairs

Establishing clear D–A junctions in COFs promotes oriented intramolecular charge separation and introducing π-conjugated structures such as alkynyl groups suppresses charge recombination which are key prerequisites for developing a competent photocatalyst. In our plot, a classical linker with C_3 symmetry (TP as an electrophilic acceptor) is allowed to form imine links with three alkyne-rich amine-terminal monomers **S1**, **S2**, and **S3** to give TP-COFs. To evaluate the possibility of a D–A junction in the selected COFs, the highest occupied molecular orbitals (HOMOs) and lowest unoccupied molecular orbitals (LUMOs) of all building blocks were calculated (Fig. 1).

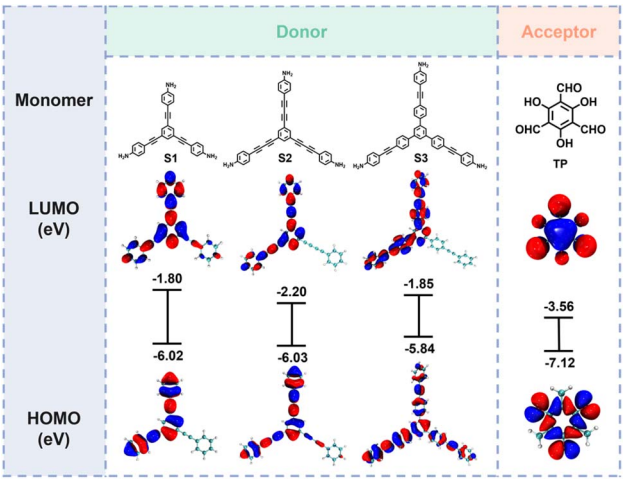

Fig. 1 HOMO and LUMO energy level diagram of building blocks for constructing the D–A junction deduced from density functional theory (DFT) using Gaussian 16A software with B3LYP/6-31G (d) as the functional and basis sets (red and blue denote positive and negative regions, isosurface values = 0.02 a.u.).

To attain the D–A junction in a system, the HOMO should be dominated by the donor while the LUMO should be mainly contributed by the acceptor.[28–30] A clear D–A junction in TP-COFs is established with the alkyne-rich building blocks and TP unit taking up the role of donor and acceptor respectively. Noteworthily, an extension of the alkynyl π system (*i.e.*, from −C≡C− in **S1** to −C≡C−C≡C− in **S2**) narrows the HOMO–LUMO gap, indicating higher conjugation in diacetylene than in the monoacetylene bridge. Therefore, TP-COFs were used as platforms to study how alkynyl π-bridges on donors modulate photocatalytic properties.

Synthesis and characterization of TP-COFs

TP-centered trialdehyde is commercially available while alkyne-bridged triamines were synthesized through Sonogashira coupling and Glaser–Hay coupling (for synthetic details, see ESI, Schemes S1, S2 and Fig. S1–S8†). Noteworthily, another common synthetic strategy to prepare linker **S2** by direct coupling between 4-ethynylaniline and 1,3,5-triethynylbenzene was found to give low selectivity and yield because of the homocoupling of 4-ethynylaniline. β-Ketoenamine-linked TP-COFs as a honeycomb net were synthesized by condensation between amines and TP in the mixture of mesitylene/1,4-dioxane/6 M acetic acid (Fig. 2a). TP-COFs were prepared smoothly by the optimized protocols notwithstanding the extension of the alkynyl π system or change of electronic conjugation in triamines. Also, **S1-TP COF** was reported in our previous work.[31]

Powder X-ray diffraction (PXRD) patterns show high crystallinity of TP-COFs (Fig. 2b and S9–S11†). Reasonable R_{wp} and R_p values (R_{wp} = 3.24–3.60% and R_p = 2.52–2.78%) based on the Pawley refinement indicate that these COFs have a 2D hexagonal network with space group of *P*6 symmetry and AA stacking mode (**S1-TP COF**: a = 23.18 Å and c = 3.52 Å; **S2-TP COF**: a =

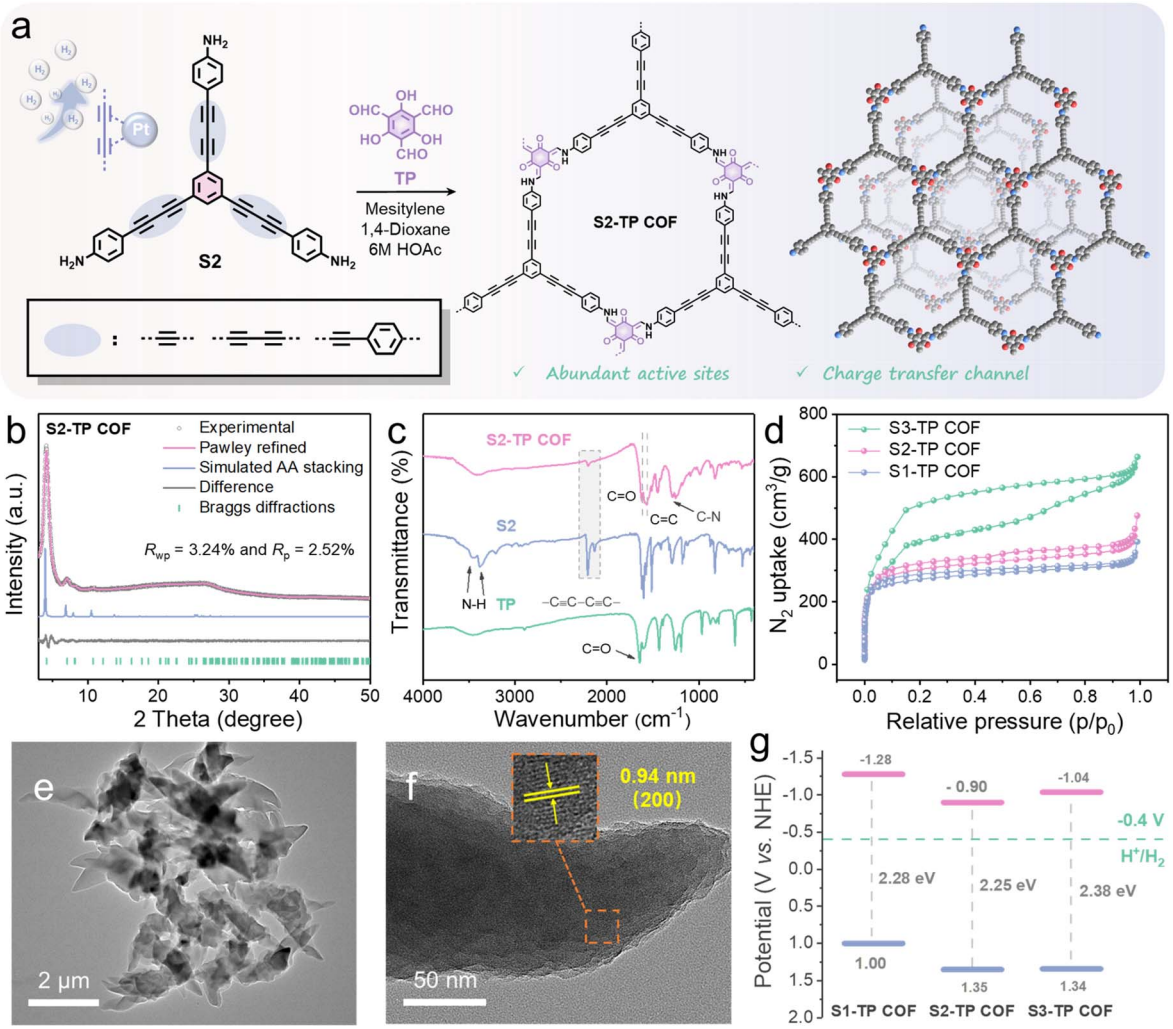

Fig. 2 (a) Molecular building blocks and structural models for TP-COFs. (b) Experimental, simulated, and Pawley refined PXRD of **S2-TP COF**. (c) FT-IR spectra of **S2-TP COF**. (d) N_2 sorption isotherms of TP-COFs. (e) HR-TEM image and (f) magnified HR-TEM image of **S2-TP COF** (orange inset shows lattice stripes corresponding to the (200) crystal plane). (g) Band structures of TP-COFs.

25.10 Å and c = 3.34 Å; **S3-TP COF:** a = 27.75 Å and c = 3.29 Å, with c referring to the interlayer spacing, Table S1†). Note that the narrower interlayer spacing from **S1-TP COF** (3.52 Å) to **S2-TP COF** (3.34 Å) probably originates from stronger interlayer π–π interaction by extending the acetylene bridge from −C≡C− to −C≡C−C≡C−. Considering the Fourier-transform infrared (FT-IR) spectra of TP-COFs, the emerging C=O stretching, C=C stretching, and C−N vibrational bands at ∼1623, 1565, and 1287 cm^{-1} together with the disappearing N−H and C=O (∼1644 cm^{-1}) signals of monomers (Fig. 2c, S12 and S13†) support the formation of the β-ketoenamine linkage *via* enol–keto tautomerization. Notably, in TP-COFs, −C≡C− stretching signals at 2207 cm^{-1} prove the chemical tolerance of dialkynyl bridges throughout the COF assembly. Besides, the β-ketoenamine linkages of **S2-TP COF** and **S3-TP COF** were verified by solid-state ^{13}C NMR spectroscopy (∼147.1, 107.7, and 184.5 ppm for the enamine carbon =C−N, α-enamine carbon C=C, and keto carbon C=O, respectively, Fig. S14 and S15†) and X-ray photoelectron spectroscopy, XPS (C−N, ∼400 eV in N 1s spectra, Fig. S16 and S17†), as was probed in previously reported **S1-TP COF.**[31] Moreover, the Raman spectra of the samples show strong signals at ∼1182 cm^{-1} and ∼2217 cm^{-1}, attributable to the in-phase stretching vibration of sp^2 hybridized carbons (=C−N) in aromatic rings and internal alkynes (Fig. S18†), respectively.

The N_2 sorption isotherms of these COFs (Fig. 2d and S19–S21†) were measured at 77 K and all of them demonstrate remarkable Brunauer–Emmett–Teller (BET) surface areas and clear pores (BET surface areas and pore sizes, obtained from non-local density functional theory (NLDFT)—**S1-TP COF**: 1054 m^2 g^{-1}, 1.73 nm; **S2-TP COF**: 1162 m^2 g^{-1}, 1.73 nm; **S3-TP COF**: 1274 m^2 g^{-1}, 2.43 nm). Note that **S1-TP COF** and **S2-TP COF** exhibit the typical type-I isotherm, indicating a microporous structure while **S3-TP COF** shows a typical type-IV isotherm with mesoporous characteristics. As shown by scanning electron microscopy (SEM), TP-COFs were clusters of submicron flakes (Fig. S22†). As shown in transmission electron microscopy (TEM) images, a lattice fringe (0.94 nm) corresponding to the (200) phase of **S2-TP COF** is visible, highlighting good

crystallinity of the COF and consolidating the appropriateness of the simulated structure (Fig. 2e and f). Notably, thermogravimetric analysis (TGA) under an N_2 atmosphere reveals high thermal stability of the TP-COFs with most of the weight (weight loss <5%) retained up to 400 °C of TP-COFs (Fig. S23†). Besides, consistent PXRD patterns of COFs before and after immersion in various solutions for 3 days indicate their satisfactory chemical stability, which is beneficial to photocatalysis (Fig. S24†).

To evaluate the feasibility of the COFs as HER photocatalysts, the optical absorption profiles and electronic band structures of the COFs were characterized using UV-visible diffuse reflectance spectroscopy (UV-Vis DRS) and Mott–Schottky (M–S) measurement. The D–A interaction leads to a red-shift in the absorption band of the D–A type COFs, and the red-shift is more obvious with stronger D–A interaction.[32] All the TP-COFs absorb strongly in the visible spectral region with obvious redshifts when compared with monomers, **S1**, **S2**, and **S3**, indicative of the successful construction of the D–A junction (Fig. S25†). Among these COFs, the GDY-like COF (COF based on **S2**) demonstrates even red-shifted absorption tailing until around 1000 nm, featuring a wider light-harvesting spectrum than COFs built from **S1** and **S3** (Fig. S25†). By Kubelka–Munk conversion, the band gaps of **S1-TP COF**, **S2-TP COF**, and **S3-TP COF** were found to be 2.28, 2.25 and 2.38 eV respectively (Fig. S26†). M–S plots reveal all the COFs to be n-type semiconductors which bear a conduction band (CB) edge lying higher than the flat-band potential by 0.1 V.[33–35] Therefore, the CB edges relative to a normal hydrogen electrode (NHE, pH = 7) of **S1-TP COF**, **S2-TP COF**, and **S3-TP COF** were calculated to be −1.28, −0.90 and −1.04 V, which are more negative than the redox potential required to drive H^+-to-H_2 reduction (−0.41 V *vs.* NHE, pH = 7) (Fig. 2g and S27†), suggesting these COFs to be suitable for the HER from the thermodynamic point of view.

Photocatalytic performance of COFs

Note that TP-COFs bearing polar keto and protic amine groups show good hydrophilicity as revealed by their small water contact angles (**S1-TP COF**: 71°; **S2-TP COF**: 54°; **S3-TP COF**: 77°, Fig. S30†) improved the hydrophobic defects of the **S2** monomer itself (Fig. S29, similar to GDY). Thanks to the hydrophilic nature, TP-COFs are suitable for systematic comparison to rationalize the function of the diacetylene bridge on photocatalysis, suppressing the HER by good H_2O flow in COF pores which enhances the accessibility of active sites. After optimization of reaction conditions, TP-COFs were used for the photocatalytic HER study under visible-light irradiation (λ > 420 nm) in a DMF/ascorbic acid (AA) mixture with Pt as a co-catalyst (Fig. 3a, S33–S40 and Tables S3–S9†). **S2-TP COF** showed a monotonic increase in H_2-evolution performance (Fig. 3b) with a higher HER rate (10.16 mmol g^{-1} h^{-1}) than **S1-TP COF** (3.71 mmol g^{-1} h^{-1}) as well as **S3-TP COF** (1.13 mmol g^{-1} h^{-1}) and this indicates that the –C≡C–C≡C– skeleton in **S2-TP COF** may exert some functions to promote the HER. Notably, **S2-TP COF** gave an unsatisfactory HER rate of 3.26 mmol g^{-1} h^{-1} in AA aqueous solution, with the amount of H_2 evolving 3-fold lower

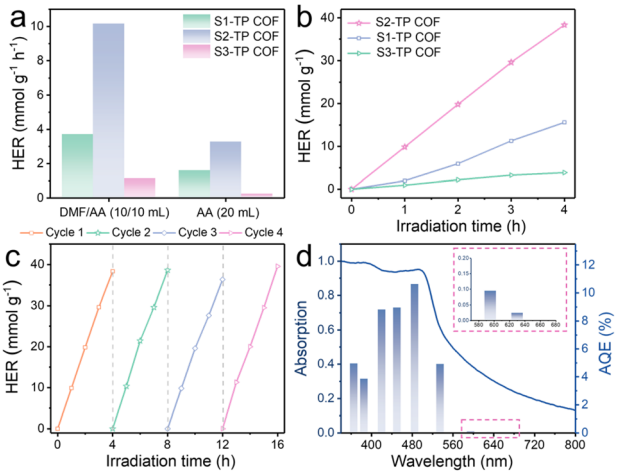

Fig. 3 (a) Photocatalytic H_2 evolution rates of TP-COFs with 3 wt% Pt feeding content. (b) Time-dependent H_2 evolution curves of TP-COFs (5 mg) with 3 wt% Pt feeding content upon visible-light illumination (λ > 420 nm). (c) Cycling stability tests of H_2 evolution (4 hours for each cycle) and (d) comparative plot between wavelength-dependent AQY and absorption profile of S2-TP COF.

than that in the mixed solvent system. As shown in Fig. S32,† TP-COFs were well dispersed (beyond 30 minutes) in the DMF/AA mixture but rapidly precipitated in the AA solution, suggesting less aggregation in the mixed system. The downsizing of TP-COFs in the DMF/AA mixture exhibited significantly enhanced H_2 evolution performance because of their increased active site exposure and light-harvesting properties.[36]

Besides, the TP-COFs demonstrate operational stability (say **S2-TP COF** maintained steady HER rates of around 10 mmol g^{-1} h^{-1} over 4 photocatalytic cycles, Fig. 3c). Moreover, consistent PXRD patterns (retained crystallinity), FT-IR spectra (unchanged chemical functionalities), and morphologies of TP-COFs before and after photocatalysis consolidate their photo- and operational stability (Fig. S41 and S42†). The best catalytic dosage was found to be 2 mg as reflected by the peak HER rate of 14.35 mmol g^{-1} h^{-1} with **S2-TP COF** (Fig. S37†); even though a higher input of the catalyst lowers the rate probably stemming from weaker light absorption by aggregation of catalysts, to minimize errors, a higher dosage of catalysts (*i.e.*, 5 mg) was used for comparing the HER performance of the COFs studied in this work. To evaluate the light utilization efficiency of the COF, the best-performing **S2-TP COF** was adopted to study the apparent quantum yield (AQY) for the HER using different band-pass filters (365–760 nm, Fig. 3d, S43 and S44†). **S2-TP COF** bearing 3 wt% Pt showed the top AQY of 10.62% upon 485-nm irradiation. The consistency between the AQY trend and absorption profile in **S2-TP COF** revealed the reliance of HER performance on photocatalysts and incident light.[37–39] It is worth noting that the AQY of **S2-TP COF** significantly falls regardless of the selected wavelength indicating the enhancement of light utilization by Pt. For comparison, 1,3,5-triethynylbenzene was adopted to construct the GDY derivative (**HGDY**) by Glaser coupling (Scheme S4†).[40] Despite the appropriate band gap (E_g = 2.25 eV, Fig. S28†), **HGDY** only gave

negligible photocatalytic HER performance (3.93 μmol g^{-1} h^{-1}) under the same conditions when compared with **S2-TP COF** (10.16 mmol g^{-1} h^{-1}). Low crystallinity of **HGDY** based on random coupling, lack of D–A junction, and hence weak charge separation in **HGDY** probably accounts for its far lower HER rate.

Mechanism insights on photocatalytic HER

To rationalize the divergence in photocatalytic activities of TP-COFs, a series of photophysical and electrochemical measurements were conducted. Electrochemical impedance spectroscopy (EIS) showed a far smaller arc radius of **S2-TP COF** than those of **S1-TP COF** and **S3-TP COF** (Fig. S45†), indicating the smallest charge transfer resistance in **S2-TP COF**. On the other hand, all TP-COFs exhibited stronger electron paramagnetic resonance (EPR) signals upon photoirradiation (Fig. 4a), revealing the formation of more unpaired electrons in **S2-TP COF** under illumination. Also, the strongest transient photocurrent response (photocurrent intensity = 0.21 μA cm^{-2}, Fig. S46†), weakest photoluminescence (λ_{ex} = 370 nm, Fig. 4b) and longest photoluminescent lifetime (Fig. 4c) of **S2-TP COF** highlight the strongest generation, the best separation/worst e^-–h^+ pair recombination and the longest lifespan of photogenerated carriers of **S2-TP COF** amongst all TP-COFs.[41–43]

Given that photoinduced e^-–h^+ dissociation is critical to photocatalytic efficiency, exciton binding energies (E_b) of TP-COFs were used to evaluate their charge recombination tendency.[44–46] By temperature-dependent fluorescence spectroscopy (77–300 K, E_b obtained by fitting emission signals of largest intensity using the Arrhenius equation, see the ESI† for fitting details), E_b values of **S1-TP COF** and **S3-TP COF** were calculated to be 78.4 and 70.9 meV respectively while that of **S2-TP COF** is the lowest at 62.8 meV (Fig. 4d–f and S47†), indicative of the most difficult e^-–h^+ recombination/effective e^-–h^+ dissociation in **S2-TP COF**. To visualize the transport of photogenerated carriers, *in situ* kelvin probe force microscopy (KPFM) was employed to observe the changes in surface potential of TP-COFs upon photoirradiation (Fig. 4g–i and S48†).[47–49] Upon illumination, **S2-TP COF** darkened the most (Fig. 4i) and gave the most negative shift of surface potential by 46.4 mV (negative

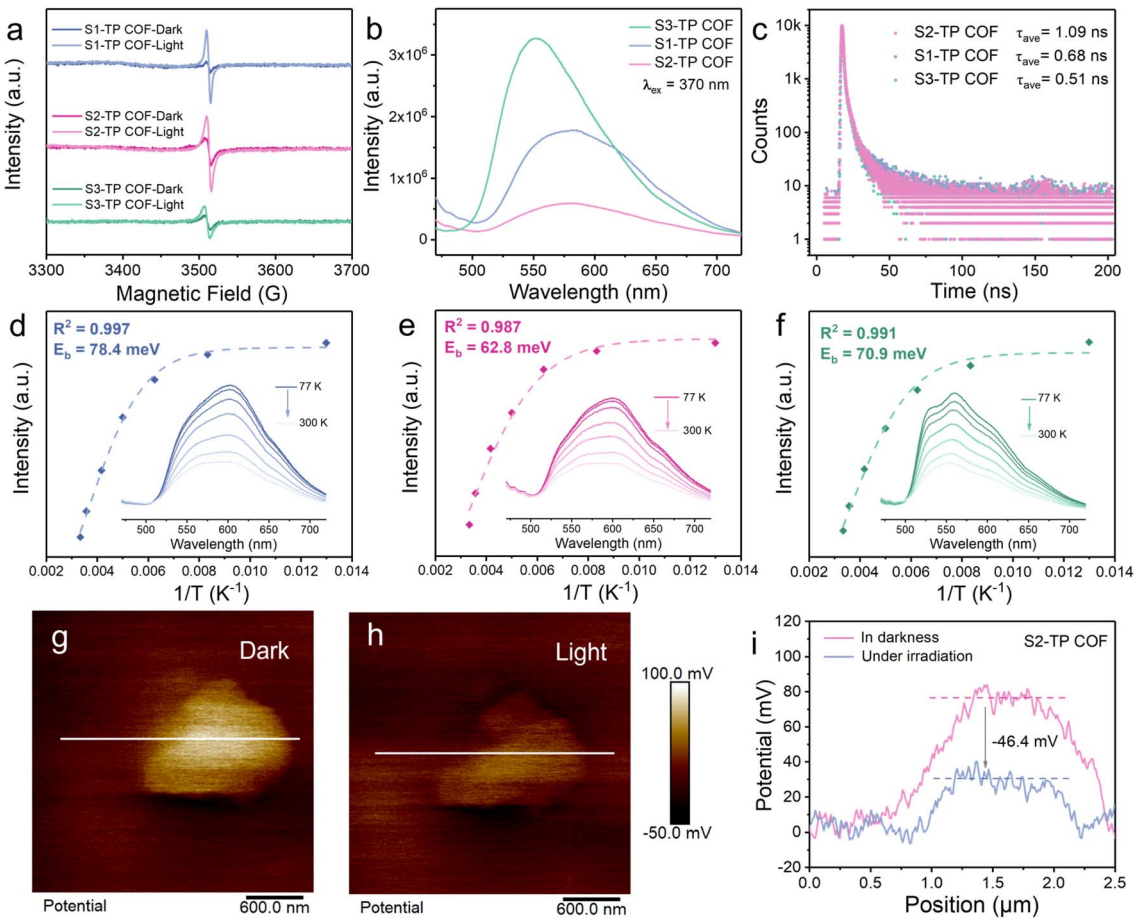

Fig. 4 (a) EPR spectra (in the dark and upon photoirradiation, measurement after 5-minute illumination), (b) room-temperature steady-state photoluminescence spectra, and (c) time-resolved fluorescence spectra (TRFS) of TP-COFs. Integrated PL intensity as a function of temperature and the fitted exciton binding energy of **S1-TP COF** (d, blue), **S2-TP COF** (e, pink), and **S3-TP COF** (f, green) (inset: temperature-dependent PL spectra from 77 to 300 K under the excitation wavelength of 370 nm). Surface potential distribution images of **S2-TP COF** (g) in darkness and (h) under UV-light irradiation, as well as (i) the corresponding surface potential difference of the cross-section of **S2-TP COF** before and after photoirradiation.

shifts of surface potential: **S1-TP COF** = 22.8 mV; **S3-TP COF** = 21.4 mV, Fig. S48d and S48l†), suggesting greater photoinduced aggregation of electrons on the surface of **S2-TP COF** than the other two analogues and indicating the strongest e^-–h^+ dissociation in **S2-TP COF**. These findings jointly highlight the best e^-–h^+ dissociation/separation in **S2-TP COF** and probably relate e^-–h^+ recombination suppression to the π-extended system, faster charge transport, and the enhanced flatness of the conjugated system through installing −C≡C−C≡C− motifs into the framework.

As Pt is a key player for the HER, detailed characterization was carried out on COFs after photocatalysis. Specifically, the energy-dispersive spectroscopy (EDS) mapping revealed a uniform distribution of C, O, N, and Pt elements (Fig. S49†), confirming the presence of Pt element in the sample of **S2-TP COF** after photocatalysis. As shown in the TEM images (Fig. S50†), numerous Pt single atoms are dispersed over the whole framework showing a corresponding lattice stripe spacing of about 0.11 nm, attributed to the (222) facet of Pt single atoms. Meanwhile, no aggregation of Pt clusters was found, demonstrating excellent dispersibility. The statistical histogram of randomly selected Pt single atoms (>100 populations) shows an average particle diameter of about 2.33 nm and a narrow size distribution consolidating the nanoscale of the Pt single atoms (Fig. S51†). To move further, XPS was adopted to probe the chemical environment of Pt, and the XPS Pt 4f spectra of TP-COFs (Fig. S52–S54†) all give signals with respect to Pt^0 ($4f_{7/2}$: ~71.8 eV; $4f_{5/2}$: ~75.3 eV) and Pt^{2+} ($4f_{7/2}$: ~73.5 eV; $4f_{5/2}$: ~77.0 eV) and importantly the C 1s spectrum shows a signal at 290.3 eV, indicative of π–π* interaction between Pt atoms and **S2-TP COF** (Fig. 5a), and probably π-back bonding from Pt d orbitals to the π* orbital of the diacetylene bridge.[40,50] Compared with the original **S2-TP COF**, the =C−N peak at 399.82 eV in the **S2-TP COF** after photocatalysis was slightly blue-shifted by 0.21 eV (Fig. 5b), indicating lower electron density of N atoms originating from the interaction between ketoenamine and Pt^{2+}.[50,51] Notably, compared with **S1-TP COF** (0.42 wt%, monoacetylene site), lower Pt loadings of **S2-TP COF** (0.29 wt%, diacetylene site) estimated by inductively coupled plasma optical emission spectroscopy (ICP-OES) (Table S10†) demonstrate that the

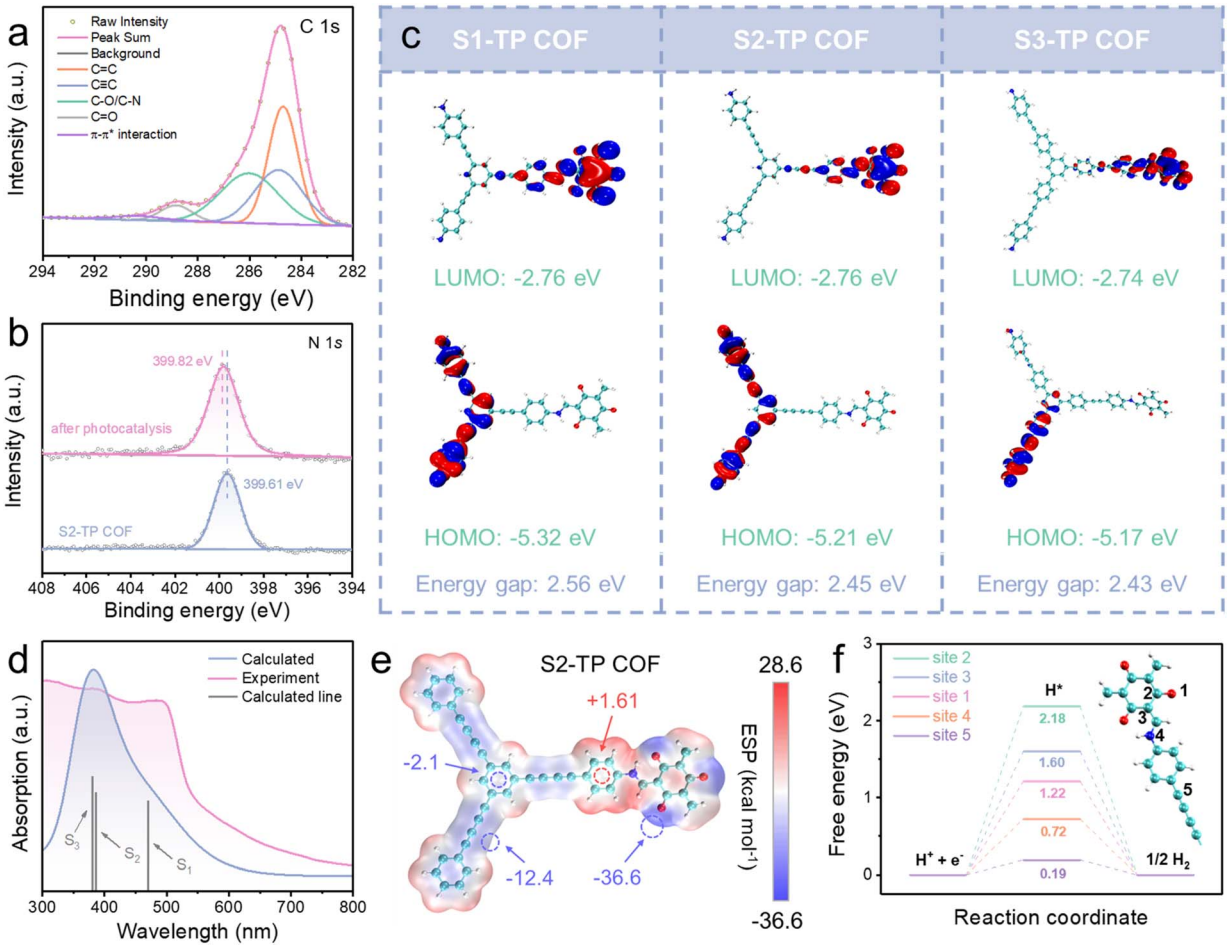

Fig. 5 (a) C 1s and (b) N 1s XPS spectra of **S2-TP COF** powder after photocatalysis. (c) HOMOs and LUMOs of the theoretical models of TP-COFs (red and blue regions denote positive and negative respectively, isosurface values of 0.02 a.u.). (d) Calculated (blue) and experimental (pink) UV-Vis absorption spectra and main vertical transitions (grey) of **S2-TP COF**. (e) Electrostatic potential maps of the **S2-TP COF** model (negative and positive regions indicated in blue and red respectively). (f) Free energy plots for selected active sites of the **S2-TP COF** model (blue, cyan, red, and white spheres represent N, C, O, and H atoms).

acetylene-rich active sites in the GDY-based framework promote the dispersion of the Pt atom, which is beneficial for the transfer of photogenerated carriers and hence HER performance.

DFT calculations

To gain more insights into charge separation and redox active sites, density functional theory (DFT) calculation at the B3LYP/6-31G(d) level was conducted on theoretical models of TP-COFs (for details of Computational procedures, see the ESI†). The Multiwfn 3.8 and VMD 1.9.3 programs were adopted to analyze orbital composition and visualization, respectively.[52,53] All atoms in the optimized models of **S1-TP COF** and **S2-TP COF** are coplanar featuring a high degree of planarity as well as electronic conjugation to exert strong interlayer π–π stacking for slower recombination and extended lifetime of excitons.[54,55] As shown in Fig. 5c, HOMOs mainly lie in **S1**, **S2**, and **S3** motifs while LUMOs centralize on the β-ketoenamine section, in agreement with the prediction of the D–A junction (Fig. 1). Non-overlapping between HOMOs and LUMOs in TP-COFs indicates good separation of photoinduced e^-–h^+ pairs which is beneficial to suppress e^-–h^+ recombination and hence improve HER efficiency. To correlate optical absorption and HER performance of TP-COFs, time-dependent density functional theory (TD-DFT) calculation was conducted using the best-performing **S2-TP COF** to scrutinize the nature of electronic transitions. As shown in Fig. 5d, the calculated absorption profile agrees well with the experimental one,[56,57] and the absorption is mainly composed of dipole-allowed $S_0 \rightarrow S_1$, $S_0 \rightarrow S_2$ and $S_0 \rightarrow S_3$ vertical transitions. Excited states S_1, S_2, and S_3 are dominantly contributed by wavefunctions of HOMO−2 → LUMO, HOMO−1 → LUMO and the linear combination of HOMO−2 → LUMO+1/HOMO → LUMO+3 respectively. Fig. S55† reveals the isosurfaces of frontier orbitals contributing to vertical transitions (HOMO−2, HOMO−1, HOMO, LUMO, LUMO+1, and LUMO+3). Noteworthily, the main contributor, HOMO−2 → LUMO, to the most allowed lowest-energy vertical transition $S_0 \rightarrow S_1$ ($\lambda_{abs} = 470$ nm) features intramolecular charge transfer (ICT) from one hand of the triazine linker to the TP core, leading to extension of light-harvesting to the visible spectral region by establishment of the D–A junction.

To elucidate the HER mechanism, potential active sites were studied by a joint experimental–theoretical approach. The best-performing **S2-TP COF** was used for *in situ* IR spectroscopic measurement to monitor any change in functionalities. In pure H_2O with Pt salt, significant weakening of −C≡C− stretching at 2215 cm^{-1} (Fig. S56†) was observed along with illumination, indicating that −C≡C−C≡C− motifs probably engage in Pt^{2+}/Pt^0 adsorption as well as formation of adsorbed hydrogen (H*) during the HER. Electrostatic potentials (ESPs) of TP-COFs of the optimized fragment structures show that electron density mainly distributes over acetylenic bridges and C=O terminals (Fig. 5e and S57†), consolidating these sites to be potential adsorption sites for Pt^{2+}/Pt^0 and H_2O.[58,59] Noteworthily, rather more even distribution of ESPs in **S3-TP COF** probably leads to less apparent charge separation (Fig. 5e) and ineffective adsorption of Pt^{2+}/Pt^0 and H_2O and these may account for the inferior HER rates.

Concerning photocatalytic HER, the Gibbs free energy change for hydrogen sorption (ΔG_{H^*}) represents a key indicator to evaluate the most energetically favorable HER active sites.[60,61] The whole profile is composed of three states: initial state ($H^+ + e^-$), intermediate state (adsorbed hydrogen, H*), and final state ($1/2H_2$) (Fig. S58†). Using **S2-TP COF** as a model, five potential active sites were locked on and found to give distinguishable ΔG_{H^*}. Importantly, the acetylene bridge (site 5) features the smallest ΔG_{H^*} (0.19 eV) suggesting site 5 to be the most kinetically favorable for the HER (Fig. 5f). Also worth noting are the imine linkage (site 4) and the keto-group (site 1) because these two sites possess smaller ΔG_{H^*} (0.72 and 1.22 eV) than the rest of the carbon-based sites (sites 2 and 3: 2.18 and 1.60 eV) (Fig. 5f), highlighting that sites 1 and 4 should not be excluded from energetically feasible HER sites. Note that considering the abovementioned ESPs (acetylene bridge and keto-group as plausible adsorption sites), both acetylene bridges and keto-groups probably serve as active sites for the HER. Experimental and theoretical evidence jointly reveals that introducing a GDY-like motif into the COF enhances HER performance by facilitating charge separation and lowering activation barriers.

Conclusions

Glaser–Hay coupling was adopted to prepare a diacetylene-bridged monomer, **S2**, which was used to construct a crystalline COF featuring a GDY-like network. By comparison with COFs built from linkers bearing a monoacetylene bridge (**S1** & **S3**), the GDY-like COF (**S2-TP COF**) indeed exhibits better charge separation, faster charge transport, and suppressed charge recombination, as exemplified by its 2.7- and 9-fold enhancement in photocatalytic HER relative to **S1-TP COF** and **S3-TP COF** respectively. This work opens an avenue to crystalline GDY mimics merging the state-of-the-art design of COFs and excellent electronic properties as well as rich easy post-synthetic modification of GDY to actualize the rational design of a high-tier sustainable photocatalyst.

Author contributions

L.-H. C., B. H., and J. H. conceived and designed the research. Z. L., S. D., and S. Y. performed the experiments and collected the data. Z. L., Q. L., and M. F. conducted the DFT calculations and analysed the data. Z. L., L.-H. C., B. H., and J. H. co-wrote the manuscript. All authors have approved the final version of the manuscript.

Conflicts of interest

There are no conflicts to declare.

Data availability

The data that support the findings of this study are available from the corresponding author upon reasonable request.

Acknowledgements

Support from the National Natural Science Foundation of China (22371054, 22301045), the Foundation of Basic and Applied Basic Research of Guangdong Province (2020B1515120024, 2024A1515012801), and Science and Technology Planning Project of Guangdong Province (2021A0505030066, 2023A0505050164) is gratefully acknowledged. We also thank the Instrumental Analysis Centre of Guangdong University of Technology for SEM images, solid-state ^{13}C NMR, EPR, and temperature-dependent and steady-state photoluminescence data collection.

Notes and references

1 G. Li, Y. Li, H. Liu, Y. Guo, Y. Li and D. Zhu, *Chem. Commun.*, 2010, **46**, 3256–3258.
2 J. Li, L. Zhu, C.-H. Tung and L.-Z. Wu, *Angew. Chem., Int. Ed.*, 2023, **62**, e202301384.
3 Y. Fang, Y. Liu, L. Qi, Y. Xue and Y. Li, *Chem. Soc. Rev.*, 2022, **51**, 2681–2709.
4 M. Wang, J. Pu, Y. Hu, Y. Zi, Z.-G. Wu and W. Huang, *Adv. Funct. Mater.*, 2024, **34**, 2308601.
5 J. Li, A. Slassi, X. Han, D. Cornil, M.-H. Ha-Thi, T. Pino, D. P. Debecker, C. Colbeau-Justin, J. Arbiol, J. Cornil and M. N. Ghazzal, *Adv. Funct. Mater.*, 2021, **31**, 2100994.
6 R. Wang, M. Shi, F. Xu, Y. Qiu, P. Zhang, K. Shen, Q. Zhao, J. Yu and Y. Zhang, *Nat. Commun.*, 2020, **11**, 4465.
7 F. Xu, K. Meng, B. Zhu, H. Liu, J. Xu and J. Yu, *Adv. Funct. Mater.*, 2019, **29**, 1904256.
8 L. Wang, Y. Wan, Y. Ding, S. Wu, Y. Zhang, X. Zhang, G. Zhang, Y. Xiong, X. Wu, J. Yang and H. Xu, *Adv. Mater.*, 2017, 1702428.
9 Z. Zhang, C. Wu, Q. Pan, F. Shao, Q. Sun, S. Chen, Z. Li and Y. Zhao, *Chem. Commun.*, 2020, **56**, 3210–3213.
10 Z. Zuo, D. Wang, J. Zhang, F. Lu and Y. Li, *Adv. Mater.*, 2019, **31**, 1803762.
11 W. Zhou, H. Shen, C. Wu, Z. Tu, F. He, Y. Gu, Y. Xue, Y. Zhao, Y. Yi, Y. Li and Y. Li, *J. Am. Chem. Soc.*, 2019, **141**, 48–52.
12 C. Bie, B. Cheng, W. Ho, Y. Li, W. Macyk, J. B. Ghasemif and J. Yu, *Green Chem.*, 2022, **24**, 5739–5754.
13 X. Liu, Y. Zhao, J. Du and D. Wang, *Sci. China Mater.*, 2024, **67**, 729–751.
14 L. Stegbauer, K. Schwinghammer and B. V. Lotsch, *Chem. Sci.*, 2014, **5**, 2789–2793.
15 Z. Yong and T. Ma, *Angew. Chem., Int. Ed.*, 2023, **62**, e202308980.
16 Z. Weng, Y. Lin, S. Guo, X. Zhang, Q. Guo, Y. Luo, X. Ou, J. Ma, Y. Zhou, J. Jiang and B. Han, *Angew. Chem., Int. Ed.*, 2023, **62**, e202310934.
17 N.-Y. Huang, Y.-T. Zheng, D. Chen, Z.-Y. Chen, C.-Z. Huang and Q. Xu, *Chem. Soc. Rev.*, 2023, **52**, 7949–8004.
18 Z. Chen, J. Wang, M. Hao, Y. Xie, X. Liu, H. Yang, G. I. N. Waterhouse, X. Wang and S. Ma, *Nat. Commun.*, 2023, **14**, 1106.
19 R. Luo, H. Lv, Q. Liao, N. Wang, J. Yang, Y. Li, K. Xi, X. Wu, H. Ju and J. Lei, *Nat. Commun.*, 2021, **12**, 6808.
20 J. Li, S.-Y. Gao, J. Liu, S. Ye, Y. Feng, D.-H. Si and R. Cao, *Adv. Funct. Mater.*, 2023, **33**, 2305735.
21 J.-N. Chang, J.-W. Shi, Q. Li, S. Li, Y.-R. Wang, Y. Chen, F. Yu, S.-L. Li and Y.-Q. Lan, *Angew. Chem., Int. Ed.*, 2023, **62**, e20230360.
22 P. Pachfule, A. Acharjya, J. Roeser, T. Langenhahn, M. Schwarze, R. Schomacker, A. Thomas and J. Schmidt, *J. Am. Chem. Soc.*, 2018, **140**, 1423–1427.
23 C.-R. Zhang, W.-R. Cui, R.-H. Xu, X.-R. Chen, W. Jiang, Y.-D. Wu, R.-H. Yan, R.-P. Liang and J.-D. Qiu, *CCS Chem.*, 2021, **3**, 168–179.
24 X.-R. Chen, W.-R. Cui, R.-P. Liang, C.-R. Zhang, R.-H. Xu, W. Jiang and J.-D. Qiu, *ACS Appl. Bio Mater.*, 2021, **4**, 6502–6511.
25 A. Khojastegi, A. Khosropour, S. Amirjalayer, I. Mosleh and A. Abbaspourrad, *Adv. Funct. Mater.*, 2023, **33**, 2309367.
26 L. A. Baldwin, J. W. Crowe, M. D. Shannon, C. P. Jaroniec and P. L. McGrier, *Chem. Mater.*, 2015, **27**, 6169–6172.
27 J. W. Crowe, L. A. Baldwin and P. L. McGrier, *J. Am. Chem. Soc.*, 2016, **138**, 10120–10123.
28 Y. Qian, Y. Han, X. Zhang, G. Yang, G. Zhang and H.-L. Jiang, *Nat. Commun.*, 2023, **14**, 3083.
29 J. Kou, G. Wang, H. Guo, L. Li, J. Fang, J. Ma and Z. Dong, *Appl. Catal., B*, 2024, **352**, 124020.
30 B. C. Deibel, T. Strobel and V. Dyakonov, *Adv. Mater.*, 2010, **22**, 4097–4111.
31 Z. Lin, Y.-H. Zhong, L. Zhong, X. Ye, L.-H. Chung, X. Hu, Z. Xu, L. Yu and J. He, *JACS Au*, 2023, **3**, 1711–1722.
32 Y. Xia, W. Zhang, S. Yang, L. Wang and G. Yu, *Adv. Mater.*, 2023, **35**, 2301190.
33 C. Han, P. Dong, H. Tang, P. Zheng, C. Zhang, F. Wang, F. Huang and J.-X. Jiang, *Chem. Sci.*, 2021, **12**, 1796–1802.
34 Z. Li, T. Deng, S. Ma, Z. Zhang, G. Wu, J. Wang, Q. Li, H. Xia, S.-W. Yang and X. Liu, *J. Am. Chem. Soc.*, 2023, **145**, 8364–8374.
35 G.-Q. Lai, Z. Jiang, H. Zhong, L.-H. Chung, N. Li and J. He, *Chin. J. Struct. Chem.*, 2023, **42**, 100090.
36 W. Zhao, L. Luo, M. Cong, X. Liu, Z. Zhang, M. Bahri, B. Li, J. Yang, M. Yu, L. Liu, Y. Xia, N. D. Browning, W.-H. Zhu, W. Zhang and A. I. Cooper, *Nat. Commun.*, 2024, **15**, 6482.
37 K. Wang, Y. Zhong, W. Dong, Y. Xiao, S. Ren and L. Li, *Angew. Chem., Int. Ed.*, 2023, **62**, e202304611.
38 Y. Wang, Z. Hu, W. Wang, H. He, L. Deng, Y. Zhang, J. Huang, N. Zhao, G. Yu and Y.-N. Liu, *Chem. Sci.*, 2021, **12**, 16065–16073.
39 Y. Luo, B. Zhang, C. Liu, D. Xia, X. Ou, Y. Cai, Y. Zhou, J. Jiang and B. Han, *Angew. Chem., Int. Ed.*, 2023, **62**, e202305355.
40 P. Zhao, H. Jiang, H. Shen, S. Yang, R. Gao, Y. Guo, Q. Zhang and H. Zhang, *Angew. Chem., Int. Ed.*, 2023, **62**, e202314121.
41 Y. Luo, C. Liu, J. Liu, X. Liu, Y. Zhou, X. Ou, B. Weng, J. Jiang and B. Han, *Chem. Eng. J.*, 2024, **481**, 148494.
42 M. Lu, S.-B. Zhang, M.-Y. Yang, Y.-F. Liu, J.-P. Liao, P. Huang, M. Zhang, S.-L. Li, Z.-M. Su and Y.-Q. Lan, *Angew. Chem., Int. Ed.*, 2023, **62**, e202307632.
43 P.-J. Tian, X.-H. Han, Q.-Y. Qi and X. Zhao, *Chem. Sci.*, 2024, **15**, 9669–9675.

44 G. Fu, D. Yang, S. Xu, S. Li, Y. Zhao, H. Yang, D. Wu, P. S. Petkov, Z.-A. Lan, X. Wang and T. Zhang, *J. Am. Chem. Soc.*, 2024, **146**, 1318–1325.
45 H. Liang, X. Bi, H. Chen, T. He, Y. Lin, Y. Zhang, K. Ma, W. Feng, Z. Ma, G. Long, C. Li, B. Kan, H. Zhang, O. A. Rakitin, X. Wan, Z. Yao and Y. Chen, *Nat. Commun.*, 2023, **14**, 4707.
46 W. Wang, H. Wang, X. Tang, J. Huo, Y. Su, C. Lu, Y. Zhang and C. Gu, *Chem. Sci.*, 2022, **13**, 8679–8685.
47 M.-L. Xu, M. Lu, G.-Y. Qin, X.-M. Wu, T. Yu, L.-N. Zhang, K. Li, X. Cheng and Y.-Q. Lan, *Angew. Chem., Int. Ed.*, 2022, **61**, e202210700.
48 Y. You, S. Chen, J. Zhao, J. Lin, D. Wen, P. Sha, L. Li, D. Bu and S. Huang, *Adv. Mater.*, 2024, **36**, 2307962.
49 R. Chen, F. Fan, T. Dittrich and C. Li, *Chem. Soc. Rev.*, 2018, **47**, 8238–8262.
50 P. Dong, Y. Wang, A. Zhang, T. Cheng, X. Xi and J. Zhang, *ACS Catal.*, 2021, **11**, 13266–13279.
51 W. Weng and J. Guo, *Nat. Commun.*, 2022, **13**, 5768.
52 T. Lu and F. Chen, *J. Comput. Chem.*, 2012, **33**, 580.
53 W. Humphrey, A. Dalke and K. Schulten, *J. Mol. Graphics*, 1996, **14**, 33.
54 K. Xiong, Y. Wang, F. Zhang, X. Li and X. Lang, *Appl. Catal., B*, 2023, **322**, 122135.
55 M. Wang, Z. Wang, M. Shan, J. Wang, Z. Qiu, J. Song and Z. Li, *Chem. Mater.*, 2023, **35**, 5368–5377.
56 Q. Zhou, Y. Guo and Y. Zhu, *Nat. Catal.*, 2023, **6**, 574–584.
57 Y. Yang, X. Chu, H.-Y. Zhang, R. Zhang, Y.-H. Liu, F.-M. Zhang, M. Lu, Z.-D. Yang and Y.-Q. Lan, *Nat. Commun.*, 2023, **14**, 593.
58 H. T. B. Pham, J. Y. Choi, S. Huang, X. Wang, A. Claman, M. Stodolka, S. Yazdi, S. Sharma, W. Zhang and J. Park, *J. Am. Chem. Soc.*, 2022, **144**, 10615–10621.
59 H. Yan, Y. Peng, Y. Huang, M. Shen, X. Wei, W. Zou, Q. Tong, N. Zhou, J. Xu, Y. Zhang, Y.-X. Ye and G. Ouyang, *Adv. Mater.*, 2024, **36**, 2311535.
60 J. Li, J. Zhou, X.-H. Wang, C. Guo, R.-H. Li, H. Zhuang, W. Feng, Y. Hua and Y.-Q. Lan, *Angew. Chem., Int. Ed.*, 2024, **63**, e202411721.
61 W. Chen, L. Wang, D. Mo, F. He, Z. Wen, X. Wu, H. Xu and L. Chen, *Angew. Chem., Int. Ed.*, 2020, **59**, 16902–16909.